Agriculture, Ecosystems and Environment 299 (2020) 106976

Contents lists available at ScienceDirect

Agriculture, Ecosystems and Environment

journal homepage: www.elsevier.com/locate/agee

Monitoring of suspended sediment load and transport in an agroforestry watershed on a karst plateau, Southwest China

Le Cao[a,b,c], Shijie Wang[a], Tao Peng[a,d,*], Qianyun Cheng[a,c], Lin Zhang[a,d], Zhicai Zhang[e], Fujun Yue[f], Alan E. Fryer[g]

[a] State Key Laboratory of Environment Geochemistry, Institute of Geochemistry, Chinese Academy of Sciences, Guiyang 550081, China
[b] Center for Lunar and Planetary Sciences, Institute of Geochemistry, Chinese Academy of Sciences, Guiyang 550081, China
[c] University of Chinese Academy of Sciences, Beijing 100049, China
[d] Puding Karst Ecosystem Research Station, Chinese Academy of Sciences, Puding 562100, China
[e] State Key Laboratory of Hydrology-Water Resources and Hydraulic Engineering, College of Hydrology and Water Resources, Hohai University, Nanjing 210098, China
[f] Institute of Surface-Earth System Science, Tianjin University, Tianjin 300072, China
[g] Department of Earth and Environmental Sciences, University of Kentucky, 101 Slone Building, Lexington, KY, 40506-0053, United States

ARTICLE INFO

Keywords:
Karst critical zone
Agroforestry watershed
Suspended sediment flux
Underground soil leakage
Rainfall regime

ABSTRACT

The timing and distribution of soil erosion in agroforestry landscapes in karst regions remains poorly understood at the watershed scale, despite the recognized deleterious impacts of soil erosion. The aim of the research presented here is to understand multi-scale soil erosion and its relationship with agricultural activities in an agroforestry catchment developed on limestone bedrock in southwest China. Soil erosion monitoring was carried out for runoff plots on the hillside of the basin, and high-frequency suspended sediment and discharge monitoring was carried out for the surface and underground rivers at the outlet of the basin. The results show that the annual sediment transport modulus in this catchment is extremely low (5.1 Mg km^{-2} a^{-1}). Sediment fluxes in the underground and surface rivers account for 19.7 % and 80.3 % of the total flux, respectively. Soil leakage is an important way but not the main way of soil erosion in this typical karst watershed. There is no obvious soil erosion on the hillsides (less than 1 Mg km^{-2} a^{-1}), and the annual soil erosion modulus in the paddy field is about 53.7 Mg km^{-2} a^{-1}. Agricultural activities dominate the distribution of soil erosion. Rainfall that generates surface runoff in the watershed is the key factor affecting soil erosion. This kind of rainfall often occurs in the summer (June to August) during crop cultivation. This study reveals that preventing soil loss from lowland farmland during heavy rainfall events should be prioritized in karst watersheds where agroforestry is practiced.

1. Introduction

Soil erosion is one of the most serious environmental problems facing human society, and it adversely affects the productivity of natural and agricultural ecosystems (Pimentel, 2006). Compared with other areas, karst areas are more prone to soil erosion, both because soil is shallow (few insoluble residues are produced after the dissolution of limestone) and because the development of solution-enhanced conduits leads to underground soil leakage (Zhang et al., 2007). Southwest China is one of the largest continuous karst areas in the world, and it is characterized by shallow surface soil, low surface runoff coefficient and high infiltration rate (Peng and Wang, 2012). This special geological condition combined with unfavorable land-use methods has led to severe soil erosion and rocky desertification (Jiang et al., 2014).

Soil erosion research in southwest China began in the 1960s. Methods used in early studies of soil and water loss were developed in the Loess Plateau area, and runoff-plot scale monitoring is the most common method of studying erosion and hydrological processes (Chen et al., 2018). Conducting continuous observations of surface runoff in six plots with different kinds of land usage on karst slopes, Tao (Peng et al., 2008) found that the surface runoff coefficient ranged from 0.01% to 12.81%, most of the rainwater flowed underground through fractures and soil pipes. Plot size is a very important factor, but there is no strong correlation between the results of studies at different scales. Raclot et al. (2009) showed that the erosion rate measured on a single farm is significantly higher than that measured on a watershed scale. Le Bissonnais et al. (1998) demonstrated that the soil loss rate was underestimated in 1–20 m^2 plots and overestimated in 20 to 500 m^2 plots. This is not only due to the connectivity of water and sediment fluxes and the difference of geomorphic response thresholds at different

* Corresponding author at: State Key Laboratory of Environment Geochemistry, Institute of Geochemistry, Chinese Academy of Sciences, Guiyang 550081, China.
E-mail address: pengtao@vip.gyig.ac.cn (T. Peng).

https://doi.org/10.1016/j.agee.2020.106976
Received 9 October 2019; Received in revised form 5 April 2020; Accepted 21 April 2020
Available online 15 May 2020
0167-8809/

scales, but also to nonlinear processes operating at various scales. As an independent hydrogeological unit, watershed-scale soil loss research can better guide agricultural activities and soil and water conservation. To our knowledge, there has yet no direct research of soil loss on watershed-scale in southwest China.

Suspended sediment in river can reflect the soil erosion in the river basin. The variation in sediment discharge is due to changes in water discharge and sediment concentration, both of which are affected by climate and human activities. Precipitation is the most important climatic factor affecting soil erosion and sediment transport (Gao et al., 2007; Zhao et al., 2015). Land-use change (human activities) is the most significant cause of soil erosion in karst areas (Kranjc, 2009). Established vegetation can prevent or minimize erosion (Niu et al., 2014). Potential evapotranspiration (PET) is closely related to water discharge, and plant growth can affect sediment transport by affecting PET and, thereby, discharge (Liu et al., 2012). However, most studies on river sediment monitoring in karst areas are based on the annual sediment transport data series, which masks the changes of river sediment in a short time scale (Wu et al., 2012; Xiong et al., 2008).

In order to understand multi-scale soil erosion of an agroforestry watershed in karst terrain and its relationship with agricultural activities, continuous observations of soil erosion in six runoff plots and high-frequency river flow and suspended sediment monitoring were carried out in a small catchment in southwest China. The objectives of this study are to understand the relationship between rainfall and sediment fluxes in surface and subsurface streams and to estimate the contribution of different land uses to soil loss.

2. Materials and methods

Chenqi catchment (26°15′44″N, 105°46′22″E) is located in Puding County, Guizhou Province. The drainage area is 1.2 km^2. The elevation is between 1316 and 1524 m above sea level, surrounded by mountains on three sides, and the average slope is about 30°. This area is a typical karst plateau peak cluster valley. The climate is subtropical humid (monsoonal). The average annual temperature is 14.3 °C (-7.6 °C–34.3 °C), the average annual rainfall is 1338 mm, and the rainfall is unevenly distributed in time and space. Precipitation during the rainy season (May–October) accounts for more than 80 % of annual rainfall. The lithology consists mainly of gently dipping carbonate rocks of the Middle Triassic Guanling Formation (inclination angle < 7°). Limestone overlies marl and shale interbeds, which form an essentially impermeable base. Groundwater tracer and water balance calculations show that the basin is essentially closed. There is a perennial surface river and three sinkholes, which are connected with an underground river. The surface/underground river outlets control the output of runoff, sediment and other materials in the basin (Peng and Wang, 2012).

Six types of land use were identified on the hillsides of the basin, including Burned Area Recovered (BAR), Burned Area Uncovered (BAU), Young Forestland (YFL), Cropland (CL), Pastureland (PL), and Combination Vegetation Land (CVL) (Table 1). Since 2007, surface runoff and soil erosion of the six types of slopes have been monitored by the large runoff field method. Concrete blocks 10 − 15 cm high are piled around six plots to prevent external runoff and sediment from entering them. A cubic tank to collect water and sediment is connected to the bottom of each plot. Table 1 shows the basic conditions of each runoff field.

A HOBO U30 small weather station (Onset Computer) was set up in BAR and CL (Fig. 1). The rain gauge is a tipping-bucket type with a resolution of 0.02 mm and a monitoring interval of 5 min. Triangular rafts were installed at the underground and surface river outlets using HOBO U20L-01 pressure transducers with a resolution of 0.02 kPa and a monitoring interval of 5 min. Measured water pressures were corrected for barometric pressure fluctuations and converted to water levels, from which flow rates were calculated using a rating curve. Turbidity is a physical optical effect that is related to the size, shape, structure and composition of the particulate matter in water (Gippel, 1995). Many scholars have argued that turbidity is an excellent indicator of sediment concentration, and it has been used in both laboratory and on-site sediment concentration measurements (Gippel, 1989; Lawler and Brown, 1992). A VisoTurb@700IQ online turbidity analyzer (WTW, Xylem Analytics) was used, and the monitoring interval was set to 5 min.

Table 1
Summary of characteristics of large runoff fields.

Fields	Land use	Slope(°)	Position	Area(m^2)	Vegetation coverage (%)	
					2007	2017
BAR	Burned (2007) Recover (2008 − 2017)	37	Upper	1255	60	80
BAU	Burned (2007) Recover (2008) Cutting (2009 − 2010) Recover (2011 − 2017)	32	Upper	684	30	75
YFL	Reforest	35	Middle	1146	85	95
CL	Tillagel	30	Foot	2440	5	75
PL	Grazing	33	Foot	2890	45	85
CVL	Wood (upper) Grass (lower)	36	Foot	2439	70	90

BAR: Burned Area Recovered; BAU: Burned Area Uncovered: YFL: Young Forestland; CL: Cropland; PL: Pastureland; CVL: Combination Vegetation Land.

According to previous research, surface water and groundwater in the Chenqi basin seldom rise under normal rainfall conditions, which may be related to the development of surface karst zones in the area (Peng and Wang, 2012). The sediment concentration of river water is generally low, which is unfavorable for the collection of sediment samples. Suspended sediment samples from surface and underground rivers were collected separately with 25L-HDPE carboys using a stainless-steel water pump over an interval of 1–2 h. The water sample was allowed to settle for about 5 days, the supernatant liquid was pumped off, the concentrated water sample was placed in a beaker and dried in an oven at 65°, and then the sediment mass was measured.

For each runoff plot, total soil erosion consists of the sum of total suspended sediment loss and total loss of coarse-grained soil. Immediately after the end of each rainfall event, the rainwater depth in the tank draining each plot was measured, the rainwater and sediment were mixed, and then they were sampled with a 2-L bottle. The remaining water inside the runoff tank was drained and the coarse soil at the bottom of the tank was weighed. The runoff samples collected in the bottles were filtered, dried, and weighed to calculate the suspended sediment concentration, which was multiplied by the corresponding runoff to calculate the total suspended sediment.

A quantitative relationship was established between turbidity and suspended sediment concentration. Previous sediment-turbidity studies have shown that there is a good linear correlation of the form (Rügner et al., 2013):

$$Y = aX + b. \quad (1)$$

In Eq. (1), X is turbidity in NTU; Y is the sediment concentration in g/m^3; a is the fit slope; and b is the fit intercept. The amount of sediment erosion for each erosive rainfall was calculated as follows:

$$M=\frac{1}{1000}\sum_{i=1}^{n}(aX + b) \times Q \times T \quad M=\frac{1}{1000}\sum_{i=1}^{n}(aX + b)*Q*T \quad (2)$$

In Eq. (2), M is the sediment mass; Q is the flow rate; T is the time interval; and n is the frequency.

Using a maximum 30-minute rainfall intensity (I_{30}, mm h^{-1}), the K-

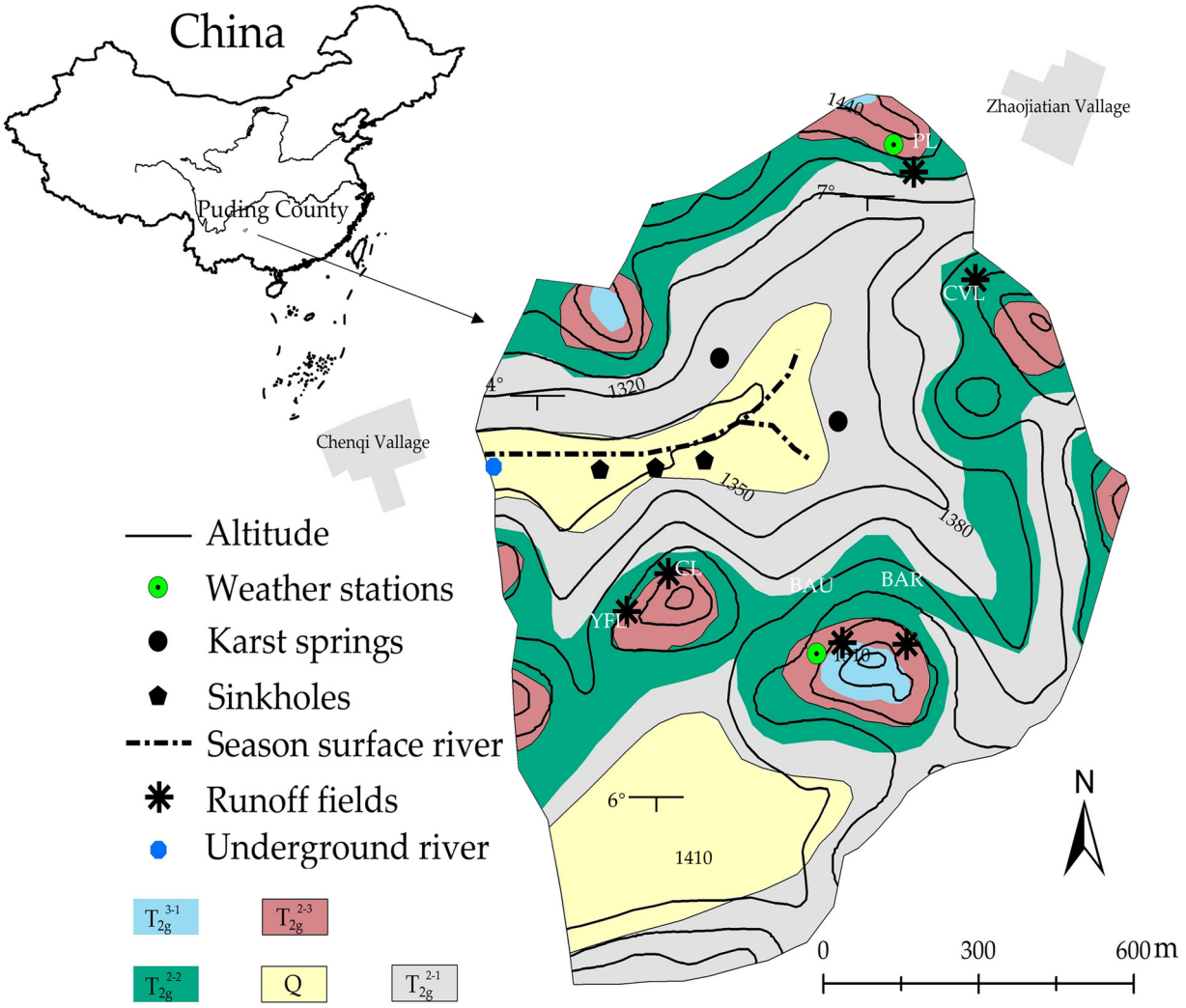

Fig. 1. Location of the Chenqi catchment. Q: Quaternary deposits; T_{2g}^{2-1}: marl intercalated with limestone of the lower part of the middle part of the middle Guanling Formation of the Middle Triassic; T_{2g}^{2-2}: limestone intercalated with marl of the middle part of the middle Guanling Formation of the Middle Triassic; T_{2g}^{2-3}: limestone of the upper part of the middle Guanling Formation of the Middle Triassic; T_{2g}^{3-1}: dolomite of the upper Guanling Formation of the Middle Triassic.

means algorithm was used to classify the rainfall in Chenqi watershed and the impact of rainfall type on surface soil erosion was evaluated. Finally, correlation analysis was used to investigate the response of surface and underground sediment transport to the characteristic indicators of rainfall (Yan et al., 2020).

3. Results

3.1. Rainfall regimes

Two weather stations in Chenqi watershed showed that the annual rainfall was 963 mm in 2017, with a peak monthly total of 284 mm in June. Based on K-mean clustering, rainfall was divided into three types (A, B and C). The test of significance showed that the classification effect is significant ($P < 0.01$). The various types of rainfall characteristics are shown in Table 2. Type A rainfall occurred twice during 2017 and averaged 78 mm with an I_{30} of 45 mm h^{-1}. A total of 17 type B rainfalls occurred in 2017, averaging 26.7 mm with an I_{30} of 19.4 mm h^{-1}. Type C rainfall averaged 4.4 mm with an I_{30} of 0.93 mm h^{-1}. Although type C rainfall had a relatively short duration (generally within 4 h) and the total for each event was relatively low, the cumulative type C precipitation was 326 mm.

Table 2
Characteristics of three types of rainfall.

Types	Fequency	P_{mean} (mm)	P_{total} (mm)	I_{mean} (mm h^{-1})	I_{30} (mm h^{-1})
A	2	78.1	156.2	8.9	45
B	16	26.7	480.6	3.9	19.4
C	74	4.4	326.2	0.93	3.2

Fequency: Frequency of rainfall in the whole year; P_{mean}: Average precipitation; P_{total}: Total precipitation; I_{mean}: Mean rainfall intensity; I_{30}: Maximum rainfall intensity in 30 min.

3.2. Runoff and sediment fluxes

The annual total runoff depth was 227 mm, including 111.3 mm for the surface river and 115.7 mm for the underground river outlet, with a catchment annual runoff coefficient of 0.24. The runoff depth associated with type A rainfall accounted for 30.7 % of the annual total runoff. Type B rainfall accounted for 54.3 % of the annual total runoff. Type C rainfall did not generate runoff.

In 2017, suspended sediment was sampled during three type B storm events (Table 3). During the three rainstorms, a total of 198 suspended sediment samples were collected with 25 L HDPE carboys. The sediment concentration was low, with an average of about 30 gm^{-3}. In order to reduce errors in sample collection, four to eight

Table 3
Sampling Information of Suspended Sediment in River Channel during Rainstorm.

Date	P (mm)	I_{30} (mm h^{-1})	T (h)	Q_{mean}(m^3 s^{-1})		C_{mean}(g m^{-3})		Samples	
				SF	UG	SF	UG	SF	UG
05/22/2017	23.4	34.8	2	0.18	0.027	25.8	12.4	8	24
06/15/2017	26.2	8.8	9	0.21	0.046	33.7	19.5	28	32
06/20/2017	50.2	12	16	0.30	0.082	38.8	25.2	56	50

P: Precipitation; T: Rainfall duration; Q_{mean}: Mean discharge; C_{mean}: Mean suspended sediment concentration; SF: Surface river; UG: Undergroud river.

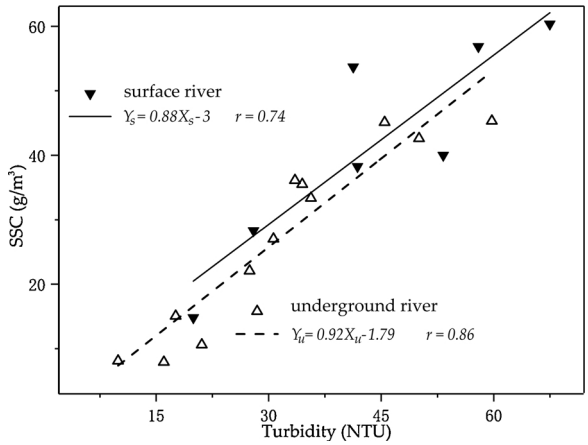

Fig. 2. Relationship between suspended sediment concentration (SSC) and Turbidity.Y_s: Surface river suspended sediment concentration, X_s: Surface river turbidity, Y_u:Underground river suspended sediment concentration, X_u : Underground river turbidity.

carboys were mixed and 19 individual data measurements were obtained. The turbidity values ranged from 10 to 60 NTU for the underground river and 20–70 NTU for the surface river. The sediment concentration ranged from 5 to 45 g m^{-3} for the underground river and 15 to 60 g m^{-3} for the surface river, and this range covers approximately 94 % of the turbidity variability that year. The correlation coefficients between the suspended sediment concentration and turbidity were 0.86 for the underground river and 0.74 for the surface river (Fig. 2).

Based on the annual continuous monitoring data of turbidity and discharge, combined with the curve of turbidity and sediment concentration, the annual sediment concentration-runoff time series was constructed (Fig. 3). Using Eq. (2), annual sediment yield was calculated: the annual sediment transport capacity of the underground river was 1.3 t and that of the surface river was 5.3 t. The annual erosion modulus of the Chenqi watershed is 5.2 t km^{-2}·a^{-1}, with the underground and surface rivers accounting for 19.7 % and 80.3 %, respectively, of sediment transport.

The characteristics of rainfall runoff and sediment transport for each erosive rainfall event and the information on total sediment transport for each type of rainfall runoff are shown in Table 4. Only eight rainfall events in the whole year, which were concentrated in June and July, resulted in sediment yield in the surface river. Type A and type B rainfall each accounted for 50 % of suspended sediment yield in the surface stream, whereas type A rainfall accounted for 27.5 % and type B rainfall accounted for 72.5 % of suspended sediment yield in the underground river. The sediment yield of 3.0 t from the two type A rainfalls accounted for 45.6 % of total annual sediment yield, whereas the 16 type B rainfalls accounted for the remaining 53.2 % of sediment yield.

3.3. Soil loss on karst limestone hill slopes

Table 5 shows the results of soil erosion modulus for six slope types during 5 different years. Pastureland (PL) exhibited the greatest soil loss each year, with a range of 0.43–69.31 Mg km^{-2} a^{-1} and a mean of 29.45 Mg km^{-2} a^{-1}. Burned Area Uncovered (BAU) exhibited the second greatest mean annual loss of soil, followed by CL; the mean annual soil loss of the other three land-use types descends in the order of CVL > BAU > YFL. Although the soil loss differed from year to year, an overall decrease in the amount of soil erosion of each slope type with time is evident (soil loss was recorded from July to December in 2007). In 2017, the soil erosion of all slopes was less than 1 Mg km^{-2} a^{-1}, and no soil loss was observed in BAU, YFL and CVL.

3.4. Response differences of surface and underground sediment yield to rainfall in karst watershed

Table 4 shows the characteristic parameters of all erosive rainfalls in 2017, including rainfall depth, average rainfall intensity, maximum 30-min intensity, rainfall erosion force, and rainfall duration. The runoff depth and suspended sediment flux of surface and underground rivers generated by each erosive rainfall are also shown in Table 4. The correlation coefficients between rainfall parameters and suspended sediment flux in both surface and underground rivers are shown in Table 6.

Except for the rainfall duration, all rainfall indicators have a strong correlation with surface river sediment mass (M_{SF}). The correlation coefficient with precipitation (P) is the highest (0.86), followed by the correlation coefficients of M_{SF} with I_{30} (0.84) and with rainfall erosion force (R, 0.81), which is a function of P and rainfall intensity. For the underground river, precipitation is still the indicator most closely related to sediment transport (M_{UD}, 0.74) and rainfall duration is least closely related (-0.15). However, the correlation coefficients between M_{UD} and the average rainfall intensity and between M_{UD} and I_{30} are only 0.36 and 0.34, respectively.

4. Discussion

4.1. Characteristics of suspended sediment flux in the karst catchment

The annual suspended sediment transport modulus of this small karst catchment is 5.1 Mg km^{-2} a^{-1}, whereas the RUSLE model erosion modulus of the 73.5-km^2 Houzhai River catchment in Puding County, to which the Chenqi catchment drains, was estimated to be approximately 170–230 Mg km^{-2} a^{-1} (Li et al., 2016). This suggests obvious differences between actual monitoring data and estimated results in karst basins. Due to the lack of support from field experiments, many parameters are commonly calculated using empirical formulas or borrowed from non-karst settings, resulting in greater uncertainty in the simulation results (Chen et al., 2018). An important difference between karst and non-karst areas is the potential for underground soil leakage or soil creeping (Zhang et al., 2007). The underground leakage of karst peak clusters was reported as more than 75 % in Guangxi Province (Jiang et al., 2014), to the south of Guizhou Province, whereas the proportion of underground soil erosion was 25 % in Chongqing karst area of Sichuan Province (Wei et al., 2015), to the north of Guizhou. In the peak-cluster depression of Guangxi Province, the proportion of underground soil leakage at the bottom of depression was 38.68 % (Luo et al., 2008). Generally speaking, although the results of underground soil leakage

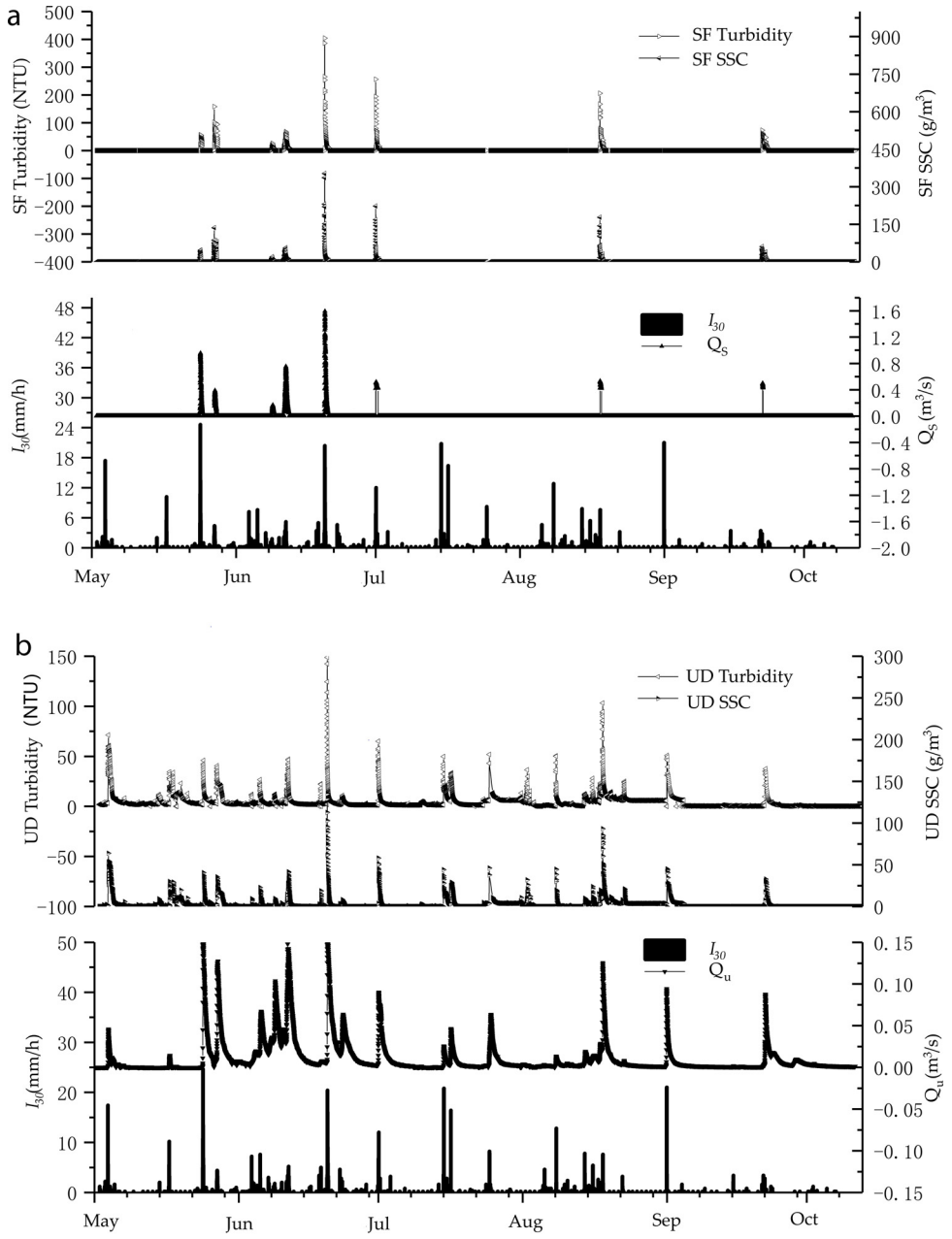

Fig. 3. Suspend sediment concentration-runoff time series. SF: Surface river, UD: Underground river, SSC: Suspend sediment concentration, I_{30}: 30-min intensity, Qs: Surface river discharge, Qu: Underground river discharge.

obtained by different researchers are different, underground soil loss is an important part of soil erosion in karst terrain.

Compared with some non-karst areas, the erosion rate is extremely low. For example, based on field sampling, the average annual sediment yield in a watershed on the northern Loess Plateau was estimated at about 17,540 Mg km^{-2} a^{-1} (Zhao et al., 2015). Some scholars have calculated the rate of soil formation under natural conditions in the southwest China karst region according to various methods. Taking the soil formation rate as the soil loss tolerance, various research results show that the allowable loss rate in karst area is 0.2–55 Mg km^{-2} a^{-1}, with an average of 4.3 Mg km^{-2} a^{-1} (Yuan and Cai, 1988; Wang et al., 1999; Jiang et al., 2010), which is comparable to the actual monitoring result (5.2 t km^{-2} a^{-1}) in this study.

4.2. Effects of rainfall on suspended sediment yield

Precipitation is the most important climatic factor affecting soil erosion and sediment transport (Gao et al., 2007; Zhao et al., 2015). Most studies indicate that rainfall intensity is closely related to soil loss. Wang (1983) pointed out that the correlation between instantaneous rainfall intensity and soil loss was the greatest among all kinds of rainfall parameters in the Loess Plateau area. In studying underground sediment erosion and karst slope erosion through simulation experiments, Yuan et al. (2016) found that rainfall intensity is positively correlated to soil loss with a correlation coefficient of 0.78. In the current study, rainfall intensity strongly affected surface soil erosion (with a correlation coefficient of 0.74), which is similar to non-karst areas. However, the impact of rainfall intensity on underground river sediment transport is not obvious (with a correlation coefficient of 0.34). The infiltration rate of rainwater depends not only on rainfall

Table 4
Characteristic parameters of each erosive rainfall.[a].

Date		Rain type	Rainfall characteristics					Sediment characteristics		Runoff characteristics	
			P	I_{30}	I	T	R	M_{UD}	M_{SF}	H_{UD}	H_{SF}
05/22		B	23.4	34.8	11.7	2	39.6	0.05	0	1.2	0
06/04		B	20.8	6	5.2	4	29.8	0.03	0	0.2	0
06/15		B	26.2	8.8	2.9	9	28.9	0.09	0.29	4.97	3.59
06/23		B	23.2	15.2	0.3	72	16.6	0.02	0	3.00	0
06/26		B	24.6	13.6	1.9	13	24.1	0.02	0.03	5.91	1.74
06/30		B	50.2	12	3.1	16	49.1	0.11	0.59	11.09	10.34
11/07		B	20.6	12.4	1.7	12	24.3	0.01	0	3.87	0
07/19		B	33.4	13.6	2.4	14	46.4	0.06	0.37	4.68	8.27
08/02		B	28.2	24.4	7.1	4	48.0	0.01	0	0.83	0
08/04		B	17.6	32.8	8.8	2	30.5	0.03	0	1.85	0
08/12		B	28	16.4	2.2	13	33.7	0.03	0	1.39	0
08/27		B	19.8	25.6	3.3	6	27.2	0.03	0	0.85	0
09/02		B	20.2	23.2	2.2	9	21.2	0.03	0	0.66	0
09/06		B	23.8	18.8	5.9	5	28.8	0.14	0.47	6.11	10.36
09/19		B	27.2	21.6	3.9	7	55.7	0.08	0	3.77	0
10/10		B	42.6	17.6	1.2	36	44.6	0.06	0.31	3.23	9.61
06/12		A	75	49.2	8.3	9	115.2	0.13	0.47	6.85	14.80
07/08		A	81.2	40.8	9.02	9	122.1	0.15	1.6	21.23	26.83
Sum	A	–	156.2	–	–	–	237.3	0.28	2.07	28.08	41.63
	B	–	480.6	–	–	–	548.5	0.80	2.06	53.56	43.91

[a] All symbols in this tables have the same meaning as the previous tables; H_{UD}: Underground river runoff depth, mm; H_{SF}: Surface river runoff depth, mm.

Table 5
Annual soil loss on limestone slopes.

Year	Annual soil loss(Mg km^{-2} a^{-1})					
	BAR	BAU	YFL	CL	PL	CVL
2007[a]	1.04	12.59	0.84	1.17	19.19	2.06
2008	0.50	4.35	0.11	9.14	69.31	3.81
2009	0.03	9.91	0.04	0.04	57.61	2.17
2010	0.04	0.10	0.06	0.05	0.43	0.02
2017	0.21	0	0	0.86	0.73	0
mean	0.36	5.39	0.21	2.25	29.45	1.61

2007[a]: Soil loss was recorded from July to December. BAR: Burned Area Recovered; BAU: Burned Area Uncovered: YFL: Young Forestland; CL: Cropland; PL: Pastureland; CVL: Combination Vegetation Land.

Table 6
Correlation coefficient between sediment discharge and rainfall characteristics.

Site	P	I_{30}	I	R	T
M_{SF}	0.86	0.84	0.74	0.80	−0.27
M_{UD}	0.74	0.34	0.36	0.71	−0.15

M_{SF}: sediment transport in surface river, Mg; M_{UD}: sediment transport in underground river, Mg; P: Precipitation, mm; T: Rainfall duration, h; I_{30}: Maximum rainfall intensity in 30 min, mm h^{-1}; I: Rainfall intensity, mm h^{-1}; R: rainfall erosion force, kJ mm h^{-1} hm^{-2}.

intensity, but also on total precipitation and underground structure.

Runoff and soil loss exhibited remarkable variances among different rainfall regimes. Peng and Wang (2012) found that large runoff and soil loss on karst slopes were mainly created by storms with a rainfall depth of more than 40 mm and an I_{30} value of over 30 mm h^{-1}. In this study, type B rainfall, which represents moderate rainfall intensity and moderate total rainfall, was the main contributor to runoff and sediment yield in Chenqi catchment. Type A rainfall, which represents high instantaneous and average rainfall intensity and high total rainfall, is similar to rainfall regimes IV and V proposed by Peng and Wang (2012). Type A rainfall is potentially the key rainfall regime impacting annual variability in sediment transport in this karst agroforestry ecosystem.

In karst environments, runoff is generated when both soil and limestone fissures and fractures are fully saturated with water. When the rainfall intensity is greater than the infiltration rates of limestone fissures and fractures, conventional saturation-excess runoff occurs (Peng and Wang, 2012). However, in low-lying paddy land, surface runoff is generated when soil is fully saturated with water. Table 6 shows that ten rainfall events, with P values between 17.6 and 28 mm and I_{30} values between 6 and 34.8 mm h^{-1}, did not generate surface runoff. In comparison, eight rainfall events, with P values between 23.8 and 81.2 mm and I_{30} values between 8.8 and 49.2 mm h^{-1}, generated surface runoff. The overlaps in P and I_{30} ranges indicate that generation of surface runoff depends on antecedent moisture conditions as well as on total event rainfall and precipitation intensity.

4.3. Agricultural activities and the distribution pattern of soil erosion

The results of runoff field monitoring in this study show that there is no risk of soil erosion on karst limestone slopes with good vegetation coverage under natural conditions. The Grain to Green Program was launched in 1999 to control soil erosion by converting sloping croplands and barren lands to forest and grassland (Tong et al., 2017). Driven by this policy, sloping farmland has been transformed into woodland and vegetation has been restored in many karst areas in southwest China. Zhang et al. (2015) found that the areas of woodland and grassland in Puding County increased by 53 % and 50 %, respectively, from 1999 to 2009. Table 1 shows the vegetation coverage of different runoff fields in the Chenqi watershed in 2007 and 2017 calculated by aerial photo interpretation. The average vegetation coverage on the slopes of the Chenqi catchment increased from 49.2%–84.2% after nearly 10 years of closing hills for afforestation. The annual erosion modulus on limestone slopes in 2008 was as high as 69.31 Mg km^{-2} a^{-1}. With the decrease of human activities and the increase of vegetation coverage, the soil erosion modulus on the slopes was less than 1 Mg km^{-2} a^{-1} by 2017 (Table 5). Considering that sediment will also accumulate along drainage pathways during transport, the slight soil erosion of the limestone slopes in Chenqi catchment basically does not contribute to the river sediment.

Because of ongoing agricultural activity, soil and water loss in the Chenqi catchment cannot be completely ignored. The labor shortage in China's rural areas has led to increased uncultivated land and hastened significant changes to traditional agricultural practices, such as reduced tillage (Yang, 2013). Table 7 shows the land-use patterns in the Chenqi catchment. Grass, shrub and forest are distributed on the hillsides and

Table 7
land-use patterns in Chenqi catchment.*.

Item	Area proportion (%)
Grass	2.4
Shrub	25.4
Forest	28.6
Dryland	34.1
Paddy field	9.5

* Data from Puding Karst Ecosystem Research Station, Chinese Academy of Sciences.

the dry land is distributed around the foot of the hills, which was used as sloping farmland before. One rice crop per year is planted on paddy fields in the flat, low-lying middle of the basin, which contains thick soil and abundant water resources. Assuming no soil erosion on the hillsides, the annual soil erosion modulus of the paddy fields, which occupy 9.5 % of the entire catchment area, is about 53.7 Mg km^{-2} a^{-1}.

5. Conclusion

This study has documented spatial and temporal variability in soil erosion in a humid, subtropical karst watershed in which agroforestry is practiced. Soil loss from six runoff plots on limestone slopes decreased with vegetation restoration between 2007 and 2017, which provided the basis for evaluating the effectiveness of afforestation strategies in soil protection. Since soil loss on the slopes is now minimal, suspended sediment in the river draining the watershed appears to originate mainly from low-lying paddy fields. Heavy rainfall events cause soil erosion on limestone slopes, but moderate rainfall ($P > 24$ mm) events can also affect soil erosion of low-lying farmland by surface runoff generation.

Underground soil leakage is a distinctive feature of soil erosion in karst areas. Research on underground soil leakage is challenging because of its concealment and complexity, and traditional soil erosion models (e.g. Universal Soil Loss Equation, USLE) need more measured data to evaluate its applicability in karst area. Monitoring of sediment transport in this study indicates underground river sediment flux contributed 19.7 % of the annual sediment flux. However, it is still necessary to use fingerprints to further determine the source of sediment transport in underground rivers. In larger karst areas with different lithological composition, clastic rock may be the main source of sediment.

Declaration of Competing Interest

We declared that we have no conflicts of interest to this work. We declare that we do not have any commercial or associative interest that represents a conflict of interest in connection with the work submitted

Acknowledgments

This work was supported by the National Key Research and Development Program of China [2016YFC0502602]; the National Natural Science Foundation of China [41571130074, U1612441, 41403112]; the “Strategic Priority Research Program” of the Chinese Academy of Sciences [XDB40020201]; and the International Partnership Project [132852KYSB20170029]. Thanks to those anonymous reviewers, who provided thoughtful comments that improved the manuscript.

References

Chen, H.S., Feng, T., Li, C.Z., Fu, Z.Y., Lian, J.J., Wang, K.L., 2018. Characteristics of soil erosion in the karst region of southwest China research advance and prospective. Res. Soil Water Conserv. 10–16 (in Chinese with English abstract).
Gao, P., Pasternack, G.B., Bali, K.M., Wallender, W.W., 2007. Suspended-sediment transport in an intensively cultivated watershed in southeastern California. CATENA 69, 239–252.
Gippel, C.J., 1989. The use of turbidimeters in suspended sediment research. Hydrobiologia 176–177, 465–480.
Gippel, C.J., 1995. Potential of turbidity monitoring for measuring the transport of suspended solids in streams. Ecohydrology 9 (1), 83–97.
Jiang, Z.C., Yang, D.S., Cao, J.H., 2010. Chinese Soil Erosion Control and Ecological Safety. Southwest Karst Volume. Science Press, Beijing (in Chinese with English abstract).
Jiang, Z.C., Luo, W.Q., Deng, Y., Cao, J.H., Qin, X.M., Li, Y.Q., 2014. The leakage of water and soil in the karst peak cluster depression and its prevention and treatment. Acta Geoscientica Sinica 2014 (05), 35–42 (in Chinese with English abstract).
Kranjc, A., 2009. History of deforestation and reforestation in the dinaric karst. Geogr. Res. 47, 15–23.
Lawler, D.M., Brown, R.M., 1992. A simple and inexpensive turbidity meter for the estimation of suspended sediment concentrations. Hydrol. Process. 6 (2), 159–168.
Le Bissonnais, Y., Benkhadra, H., Chaplot, V., Fox, D., King, D., Daroussin, J., 1998. Crusting, runoff and sheet erosion on silty loamy soils at various scales and upscaling from m2 to small catchments. Soil Tillage Res. 46, 69.
Li, Y., Bai, X.Y., Zhou, L.Qin, Tian, X., Tian, Y., Li, P., 2016. Spatial–Temporal evolution of soil Erosion in a typical Mountainous Karst Basin in SW China, Based on GIS and RUSLE. Arab. J. Sci. Eng. 41, 209–221.
Liu, Y., Fu, B., Lü, Y., Wang, Z., Gao, G., 2012. Hydrological responses and soil erosion potential of abandoned cropland in the Loess Plateau, China. Geomorphology 138, 404–414.
Luo, W.Q., Jiang, Z.C., Hang, Q.Y., Cao, J.H., Pei, J.G., 2008. Soil distribution and Erosion characteristics in different geomorphological sites of karst peak cluster depression. Soil Water Conserv. China 2008 (12), 46–49 (in Chinese with English abstract).
Niu, R., Du, B., Wang, Y., Zhang, L., Chen, T., 2014. Impact of fractional vegetation cover change on soil erosion in Miyun reservoir basin, China. Environ. Earth Sci. 72, 2741–2749.
Peng, T., Wang, S., 2012. Effects of land use, land cover and rainfall regimes on the surface runoff and soil loss on karst slopes in southwest China. CATENA 90, 53–62.
Peng, T., Wang, S.J., Zhang, X.B., Rong, L., Chen, B., Yang, T., 2008. Results of preliminary monitoring of surface runoff coefficients for karst slopes. Earth Environ. 2008 (02), 125–129 (in Chinese with English abstract).
Pimentel, D., 2006. Soil Erosion: a food and environmental threat: environment. Dev. Sustain. 8, 119–137.
Raclot, D., Le Bissonnais, Y., Louchart, X., Andrieux, P., Moussa, R., Voltz, M., 2009. Soil tillage and scale effects on erosion from fields to catchment in a Mediterranean vineyard area. Agric. Ecosyst. Environ. 134, 201–210.
Rügner, H., Schwientek, M., Beckingham, B., Kuch, B., Grathwohl, P., 2013. Turbidity as a proxy for total suspended solids (TSS) and particle facilitated pollutant transport in catchments. Environ. Earth Sci. 69, 373–380.
Tong, X.W., Wang, K.L., Yue, Y.M., Brandt, M., Liu, B., Zhang, C.H., Liao, C.J., Fensholt, R., 2017. Quantifying the effectiveness of ecological restoration projects on long-term vegetation dynamics in the karst regions of Southwest China. Int. J. Appl. Earth Obs. Geoinf. 54, 105–113.
Wang, W.Z., 1983. Study on relations between rainfall characteristics and loss of soil in loess region. Bull. Soil Water Conserv. 1983 (04), 7–13 (in Chinese with English abstract).
Wang, S.J., Ji, H.B., Ouyang, Z.Y., Zhou, D.Q., Zhen, L.P., Li, T.Y., 1999. Preliminary Study on weathering and pedogenesis of carbonate rock. Sci. China (Series D: Earth Sciences) 572–581.
Wei, X.P., Xie, D.T., Ni, J.P., Su, C.X., 2015. Soil Erosion and loss on slope in Karst Valley Area, Chongqing with ^{137}Cs. J. Basic Sci. Eng. 23 (03), 462–473 (in Chinese with English abstract).
Wu, C.S., Yang, S.L., Lei, Y., 2012. Quantifying the anthropogenic and climatic impacts on water discharge and sediment load in the Pearl River (Zhujiang), China (1954–2009). J. Hydrol. (Amst) 452–453, 190–204.
Xiong, Y.L., Zhang, K.L., YANG, G.X., Gu, Z.K., 2008. Change in characteristics of runoff and sediment in the Wujiang River. Ecol. Environ. 17 (05), 1942–1947 (in Chinese with English abstract).
Yan, H., Zhang, J., Zhou, N., Li, M., 2020. Application of hybrid artificial intelligence model to predict coal strength alteration during CO_2 geological sequestration in coal seams. Sci. Total Environ. 711, 135029.
Yang, X.J., 2013. China’s rapid urbanization. Science 342, 310.
Yuan, D.X., Cai, G.H., 1988. Karst Environment. Chongqing press, pp. 1–332 (in Chinese).
Yuan, Y.F., Dai, Q.H., Li, C.L., Peng, X.D., 2016. Response of soil Erosion in simulated condition rainfall on typical slope farmland in karst. J. Soil Water Conserv. 2016 (03), 24–28 (in Chinese with English abstract).
Zhang, X.B., Wang, S.J., He, X.B., Wang, Y.C., He, Y.B., 2007. Soil creeping in weathering crusts of carbonate rocks and underground soil losses on karst slopes. Earth Environ. 2007 (03), 202–206 (in Chinese with English abstract).
Zhang, T., Si, H., Xu, Y.L., Xue, J.H., Chu, J., Di, Q.H., 2015. Quantitative evaluation of the impact of returning farmland to forests on land use landscape patterns in karst regions. J. Beijing Fore Univ. 37 (03), 34–43 (in Chinese with English abstract).
Zhao, G., Klik, A., Mu, X., Wang, F., Gao, P., Sun, W., 2015. Sediment yield estimation in a small watershed on the northern Loess Plateau, China. Geomorphology Amst. (Amst) 241, 343–352.

Update

Agriculture, Ecosystems and Environment

Volume 312, Issue , 1 June 2021, Page

DOI: https://doi.org/10.1016/j.agee.2020.107275

Agriculture, Ecosystems and Environment 312 (2021) 107275

Contents lists available at ScienceDirect

Agriculture, Ecosystems and Environment

journal homepage: www.elsevier.com/locate/agee

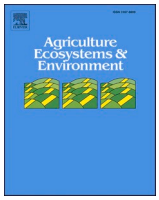

Corrigendum

Corrigendum to "Monitoring of suspended sediment load and transport in an agroforestry watershed on a karst plateau, Southwest China" [Agric. Ecosyst. Environ. 299 (September) (2020) 106976]

Le Cao [a,b,c], Shijie Wang [a], Tao Peng [a,d,*], Qianyun Cheng [a,c], Lin Zhang [a,d], Zhicai Zhang [e], Fujun Yue [f], Alan E. Fryer [g]

[a] State Key Laboratory of Environment Geochemistry, Institute of Geochemistry, Chinese Academy of Sciences, Guiyang, 550081, China
[b] Center for Lunar and Planetary Sciences, Institute of Geochemistry, Chinese Academy of Sciences, Guiyang, 550081, China
[c] University of Chinese Academy of Sciences, Beijing, 100049, China
[d] Puding Karst Ecosystem Research Station, Chinese Academy of Sciences, Puding, 562100, China
[e] State Key Laboratory of Hydrology-Water Resources and Hydraulic Engineering, College of Hydrology and Water Resources, Hohai University, Nanjing, 210098, China
[f] Institute of Surface-Earth System Science, Tianjin University, Tianjin, 300072, China
[g] Department of Earth and Environmental Sciences, University of Kentucky, 101 Slone Building, Lexington, KY, 40506-0053, United States

The authors confirms that his name was misspelled and the correct name is Alan E. Fryar.

The authors would like to apologise for any inconvenience caused.

DOI of original article: https://doi.org/10.1016/j.agee.2020.106976.
* Corresponding author at: State Key Laboratory of Environment Geochemistry, Institute of Geochemistry, Chinese Academy of Sciences, Guiyang, 550081, China.
E-mail address: pengtao@vip.gyig.ac.cn (T. Peng).

https://doi.org/10.1016/j.agee.2020.107275

Available online 19 February 2021